



Length Scale of Photospheric Granules in Solar Active Regions

Yan-Xiao Liu¹ , Chao-Wei Jiang¹ , Ding Yuan¹ , Ping-Bing Zuo¹ , and Wen-Da Cao^{2,3} 

¹Institute of Space Science and Applied Technology, Harbin Institute of Technology, Shenzhen 518055, China; chaowei@hit.edu.cn

²New Jersey Institute of Technology, Center for Solar Research, Newark, NJ, USA

³Big Bear Solar Observatory, 40386 North Shore Lane, Big Bear City, CA, USA

Received 2022 January 3; revised 2022 May 7; accepted 2022 May 25; published 2022 July 15

Abstract

Investigating the length scales of granules could help understand the dynamics of granules in the photosphere. In this work, we detected and identified granules in an active region near disk center observed at wavelength of TiO (7057 Å) by the 1.6 m Goode Solar Telescope (GST). By a detailed analysis of the size distribution and flatness of granules, we found a critical size that divides the granules in motions into two regimes: convection and turbulence. The length scales of granules with sizes larger than 600 km follow Gauss function and demonstrate “flat” in flatness, which reveal that these granules are dominated by convection. Those with sizes smaller than 600 km follow power-law function and behave power-law tendency in flatness, which indicate that the small granules are dominated by turbulence. Hence, for the granules in active regions, they are originally convective in large length scale, and directly become turbulent once their sizes turn to small, likely below the critical size of 600 km. Comparing with the granules in quiet regions, they evolve with the absence of the mixing motions of convection and turbulence. Such a difference is probably caused by the interaction between fluid motions and strong magnetic fields in active regions. The strong magnetic fields make high magnetic pressure which creates pressure walls and slows down the evolution of convective granules. Such walls cause convective granules extending to smaller sizes on one hand, and cause wide intergranular lanes on the other hand. The small granules isolated in such wide intergranular lanes are continually sheared, rotated by strong downflows in surroundings and hereby become turbulent.

Key words: Sun: granulation – Sun: photosphere – Sun: faculae – plages

1. Introduction

Granules in the solar photosphere are highly dynamic and turbulent characterizing by random motions and large Reynolds numbers (Petrovay 2001). Investigating the sizes of granules could help understand the dynamics of granules and the interaction between granules and magnetic fields (Salucci et al. 1994; Caroli et al. 2015). The sizes of granules have been greatly studied, e.g., Roudier & Muller (1986) analyzed the perimeter (P) and area (A) relationship of $P \sim A^{D/2}$ and found the fractal dimension values D of 1.25 and 2.15 for the granules with size smaller and larger than $1''37$, respectively. The fractal dimension measures the shape irregularity of features (Lovejoy 1982), and the values D of $\frac{5}{3}$ for isotherms (Mandelbrot 1977) and of $\frac{4}{3}$ for isobars (Lovejoy 1982) are predicted for turbulence. Hence, Roudier & Muller (1986) concluded that the small granules are turbulent origins. Abramenko et al. (2012) found that the “dominant” granules with sizes larger than 1000 km show “flat” in flatness, and the mini granules with sizes smaller than 600 km demonstrate power law tendency. Flatness defined as the fourth order moment, namely kurtosis, is used to measure the intermittency of features (Abramenko 2005; Abramenko & Yurchyshyn 2010).

The intermittency demonstrates the degree how much the measured signals or variables deviate from the Gauss distribution, and is the typical character of turbulence. If the flatness behaves “flat” in a certain length range, no intermittency happens in this length range, while if the flatness demonstrates power law in logarithm coordinates, strong intermittency happens. Hereby, Abramenko et al. (2012) concluded that large granules are not intermittent but the small granules are highly intermittent. Liu et al. (2021) did the same work by using a new granule segmenting method. They fitted the size distribution by Gauss, the combination of Gauss and power-law, and power-law separately in three different length ranges, and detected two critical points to separate the granules into three regimes. According to their conclusion, the granules during their lifetimes experience convection, mixing motions of convection and turbulence, and turbulence.

Actually the size distributions and flatness applied in Abramenko et al. (2012) and Liu et al. (2021) was originally used in hydrodynamics. The fluid motions in hydrodynamics include laminar flows and turbulent flows. The laminar flows move with smooth paths in layers and the fluid elements in each layer do not mix with adjacent layers, thus they have averagely stable or constant values for variables. In other

words, the increments of these variables are averagely zero and their probability density functions are typically Gauss functions. While the turbulent flows are characterized by eddies or swirls and do not have such characteristics. In the cascading process, the energy is transferred from large eddies to small ones and the probability density functions of variables are typically power-law. In the solar photosphere, the flows are weakly ionized, and it could be roughly considered as a hydrodynamics system in granular scale. Therefore, the methods of investigating the dynamics of fluids, such as probability density functions, flatness and so on, could also be used in the solar photosphere.

The sizes of granules in quiet regions have been well investigated, while those in active regions behave differently owing to the presence of strong background magnetic fields. For instance, granules in plages are found to have smaller sizes, lower intensity contrasts and are thus called abnormal granules (Dunn & Zirker 1973; Title et al. 1992; Narayan & Scharmer 2010). They are also found to be prevented and suppressed from expansion when appearing near strong magnetic field concentrations, or extending in certain directions. The physical reason for these dominant behaviors is likely the interaction with magnetic fields, which is a very common phenomenon in solar surface, especially in active regions and magnetic network. However, the interplay in between is currently not well understood.

Because the granules in active regions manifest smaller sizes than those in quiet regions, their size distributions might be different, which further reveal a different dynamical process. Investigating the sizes of granules in active regions could help us understand the dynamical process as well as the interaction with magnetic fields. By considering this, we analyze the size distribution and flatness of granules in an active region. In this work, we first segment granules, analyze the histogram and flatness of granules in the full length range, and find a critical size separating the dynamical motions of granules into two regimes: convection and turbulence. This paper is organized as follows: Section 2 describes the observations and data processing, Section 3 presents the results and Section 4 gives discussions, and Section 5 gives a conclusion of this work.

2. Observations and Data Processing

The data were taken by the 1.6 m Goode Solar Telescope (GST) (Cao et al. 2010; Goode & Cao 2012) at wavelength of TiO 7057 Å on 2015 June 18 in Big Bear Solar Observatory (BBSO). The scientific observation target was granules near the active region NOAA 12369. The effective field of view is $59'' \times 59''$. In this region, only a few pores were included while the sunspots were not. The whole observation was taken under a very good seeing condition with the assistance of adaptive optics (Cao et al. 2010; Shumko et al. 2014). This allows the spatial resolution of GST close to $0''.1$. The reconstructed

images (Wöger & von der Lühe 2007) own a pixel size of $0''.034$ and a sample is presented in Figure 1. The high quality data allow us to extract and analyze the small scale features like granules.

We segment and classify granules by using the method described in Liu et al. (2021) which is proved to be accessible to both large bright and small faint granules. Three steps are included to extract and identify granules, namely granular edge detection, separation of closely connecting granules and distinguishing granule cells from none-granule features. Here, we briefly describe these steps, and for more details we refer to Liu et al. (2021).

- (1) Granular edge detection. Local intensity valleys as granular edges in either x or y or diagonal directions are first detected. Most of local intensity valleys are in dark granule lanes, but a few of them are on bright granules where intensities initially decrease. Thus, false edges are included, and they are discarded if their intensities are higher than $\mu + \sigma$ or if their sizes are smaller than a threshold, like 200 pixels (roughly about 139 km in diameter). μ and σ here are the mean value and standard deviation of the intensity in the whole region. After this step, the edges are generally detected. One target isolated by detected edges is labeled as a blob. Most blobs contain only one single granule, but a few of them contain multiple ones. Some granules due to staying very close to each other and sharing common edges are mistakenly segmented as individual ones. Moreover, the intensity fluctuations blur the edges, which cause these granules hard to be segmented by using the locally intensity valleys or other methods like intensity thresholds and intensity gradient thresholds. Here, we use the operation morphology to find the common edges and separate the closely connecting granules.
- (2) Separation of closely connecting “granules.” To separate the closely connecting “granules,” we start to look into every detected blob and to judge if it contains multiple “granules.” If a blob separates into two or more smaller ones after one or two times erode operations, this blob is considered to contain more than one “granule.” Otherwise, it contains an individual one. For the blobs containing multiple “granules,” the common edges are detected by implementing the eroding and dilation operations, and the closely connecting “granules” are separated directly by cutting the common edges. These segmented “granules” actually include real granules and some none-granule features, like bright points (BPs), filigrees, and clusters. We need to remove these features from granules.
- (3) Distinguishing granules from none-granule features. The none-granule features such as BPs, filigrees, and clusters (see the bright regions in panel (c) of Figures 2 and 3) are considered to be reliable tracers of flux tube footpoints in

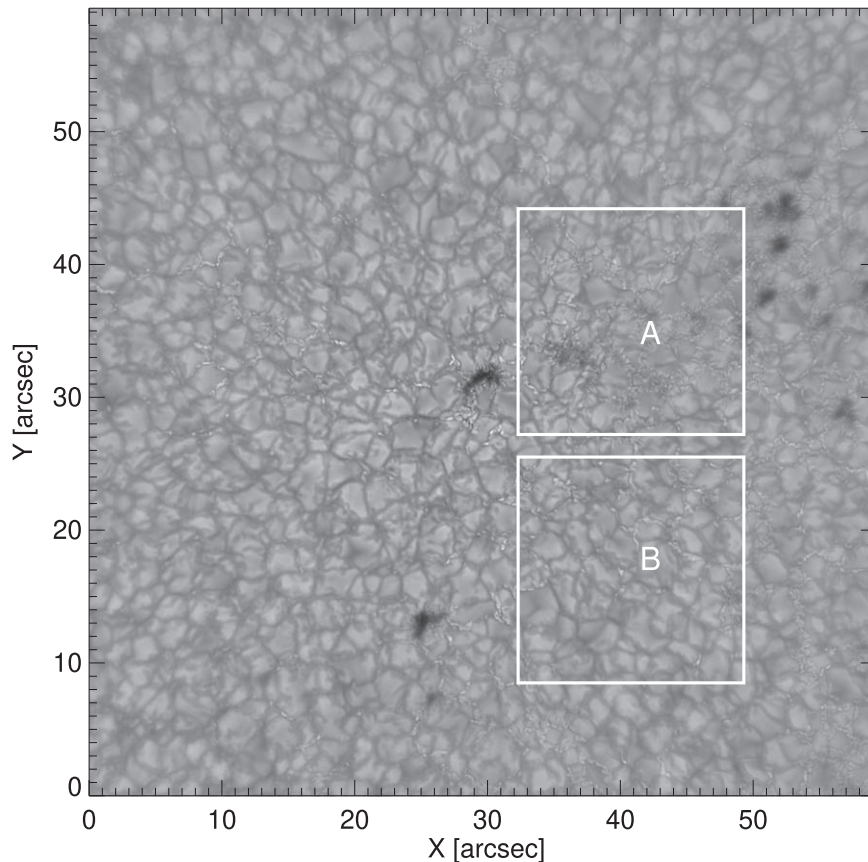


Figure 1. The original data. The two white squares mark the selected regions A and B, respectively.

the photosphere (Berger & Title 2001; Yang et al. 2015, 2016) which are characterized by strong intensity contrast and large intensity gradients (Utz et al. 2009; Liu et al. 2018). Filigrees are bright features in magnetic network regions (Dunn & Zirker 1973), and clusters are relatively large sizes of magnetic knots and usually consist of a few gathering BPs (Andic et al. 2011; Bellot Rubio & Orozco Suárez 2019). Because filigrees and clusters are actually gathering of BPs, we simply describe the steps of distinguishing granules from BPs. In this work, we take the BP identification method described in Liu et al. (2018). But the details of distinguishing BPs from bright granules is slightly different. Here, the bright granules is discarded from BPs by size thresholds rather than lifetimes. BP seeds are first selected, and then region grow is taken for every BP seed on images that only containing the newly segmented cells obtained by step (1). The derived sizes of real BPs are slightly larger than the sizes of their seeds, however, the bright granules have larger sizes after taken region grow operation. A proper size threshold is chosen to distinguish real BPs from the bright granules. When all the BPs are extracted and

identified, they are further discarded from the segmented blobs. With these three steps, the granules could be successfully segmented and identified. Here we give regions A and B as samples to present the granule segmentation and identification steps in Figures 2 and 3.

3. Results

In this work, we segmented granules in an active region with FOV of $59'' \times 59''$, which contains a few pores, plage regions, network like regions, and relatively quiet regions. We selected a plage region and a network like region as samples to analyze the granular patterns and the effect of interplay with different background magnetic fields. We extracted 9823, 834 and 795 granules in the whole FOV, in regions A and B, respectively, and their area coverage is 62%, 39% and 62%, respectively. The area coverage in region B is the same with that in the whole region, while that in region A is much less. According to Figure 1, region A contains quite a lot BPs and a few pores, which indicates that strong and dense clusters form in this region. Region B only contains some isolated and chain like BPs, which reveals that clusters are sparse comparing with those in region A. The granules

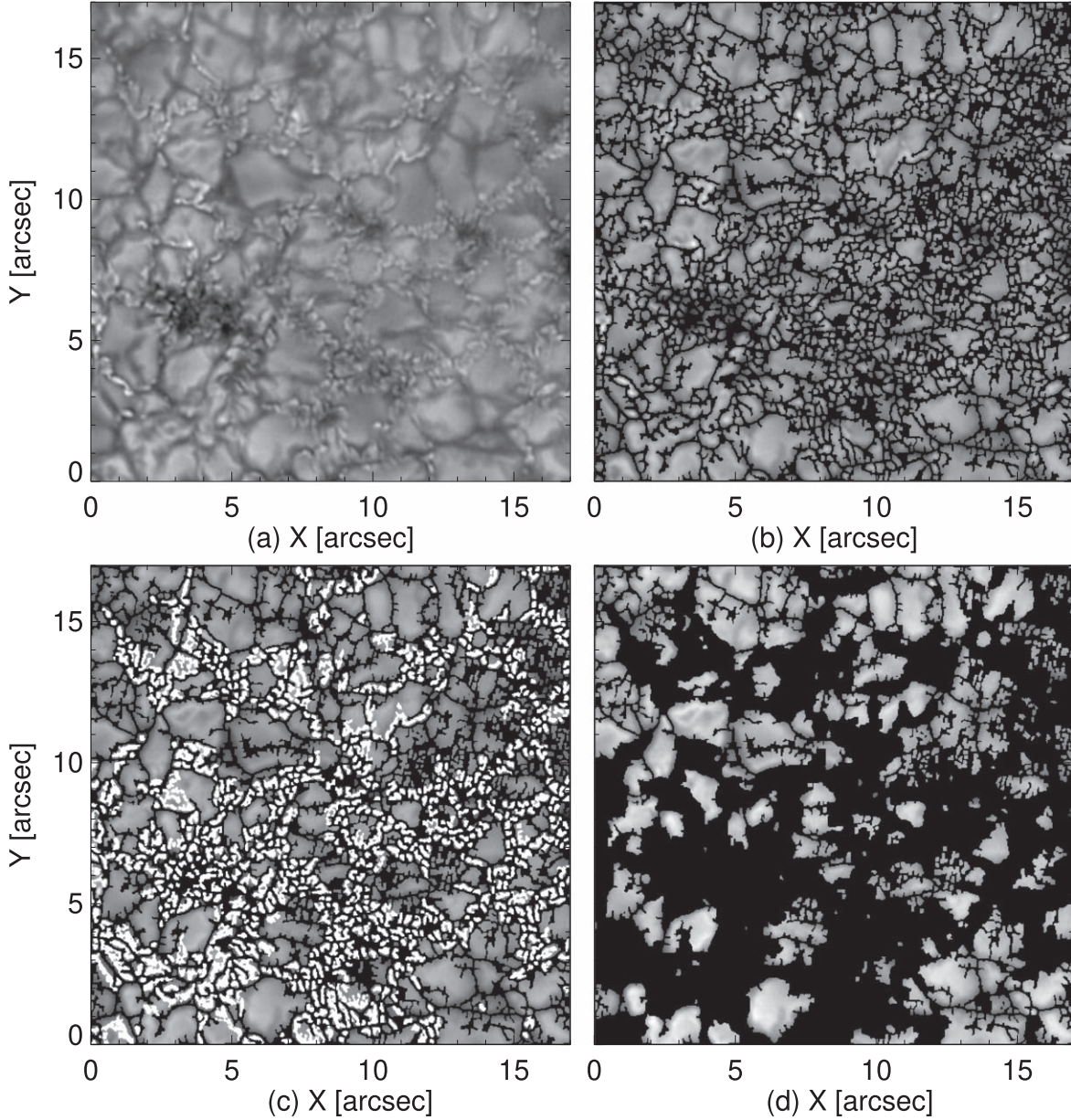


Figure 2. The granule segmentation and classification steps for Region A. Panels (a)–(d) are the original image, the segmentation result, the highlighted bright points and identified granules, respectively.

in region B appear averagely larger than those in region A. We also notice that two granules that appear in locations $[10'', 14'']$ and $[15'', 14'']$ are fully surrounded by BPs, and their borders are hereby determined, which are good examples demonstrating the interplay between granules and strong magnetic fields in morphology.

The lengths, r , of granules are calculated by assuming the granule being a circular disk and obtained directly by counting the area A ($r = 2\sqrt{A/\pi}$). The size distribution of granules in the whole region is presented in panel (a) of Figure 4 in

logarithm coordinates. It is divided into two parts by a value of $d = 600$ km. For the granules with sizes in the range of 600 km to 120 km, it is fitted by a power-law function with the slope of -1.78 and the fitting of goodness χ^2 of 0.01. For large granules with sizes above 600 km, it is fitted by a Gauss function with mean μ , standard deviation σ and the fitting of goodness χ^2 values of 123 km, 734 km, 0.02, respectively.

We also calculated the flatness, $F(r)$, for the granules in the whole region. The flatness is initially defined by the ratio of the fourth order structure function to the square of the second order

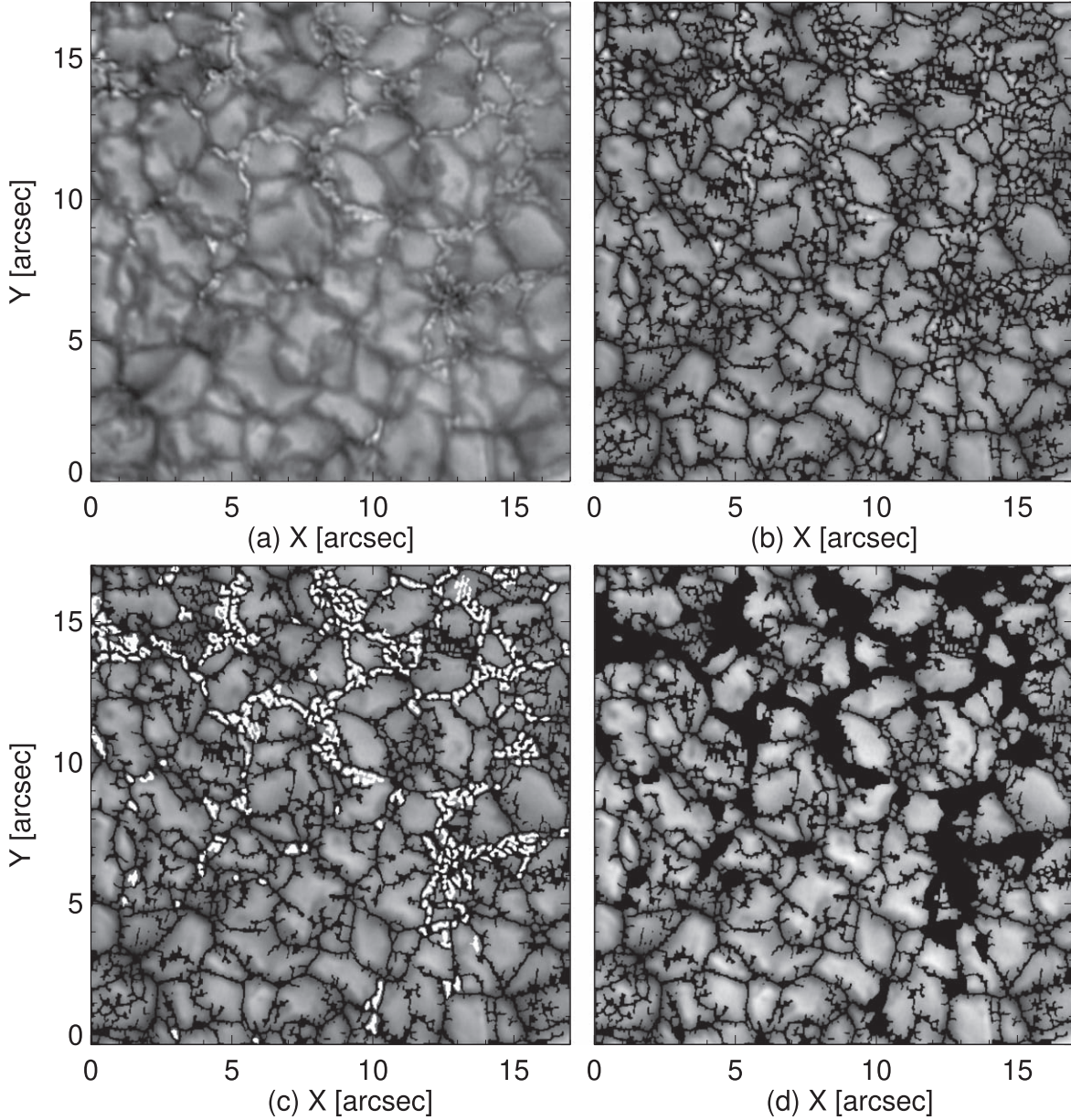


Figure 3. The same granule segmentation steps as Figure 2 but for Region B.

structure function. The q order structure function here is defined by $S_q(r) = |I(x+r) - I(x)|^q$, where I is the intensity at the location $x+r$ and x , r is the length between two pixels $x+r$ and x . Usually, a slightly higher order flatness function is suggested because it could demonstrate more details (Abramenko 2005; Abramenko & Yurchyshyn 2010; Abramenko et al. 2012). We follow the suggestion and use the sixth order flatness function here:

$$F(r) = \frac{\langle (I(x+r) - I(x))^6 \rangle}{(\langle (I(x+r) - I(x))^2 \rangle)^3}, \quad (1)$$

The flatness measures the intermittency of fluids. If the flatness behaves horizontal tendency or “flat” (hereafter “flat”) in logarithm coordinates in specific length range, the variable increment $\delta I = I(x+r) - I(x)$ for each r in this length range demonstrates the same Gauss distribution. This reveals that no intermittency happens in this length range. If the flatness function shows power-law in logarithm plots, the increment of the variable also deviates from the Gauss distribution obviously, and strong intermittency happens. In Figure 4, the flatness shows “flat” for granules with sizes larger than 600 km and behaves linearly with a negative slope of -0.82 for

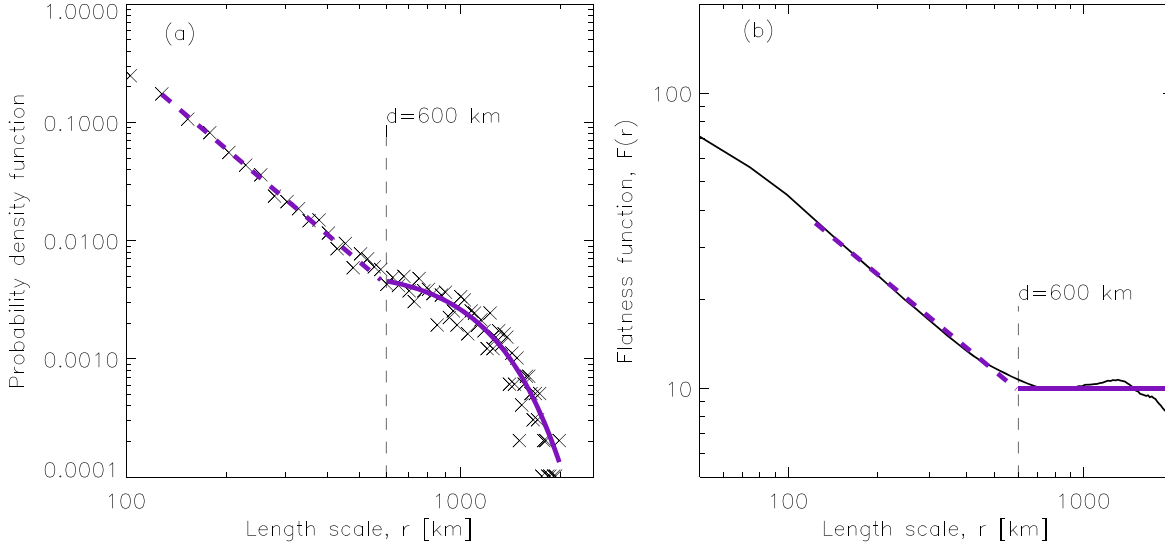


Figure 4. Size histogram and flatness of granules for the whole region. Panel (a) draws the histogram, and the dashed and solid lines in purple are the power law and Gauss function fittings, respectively. Panel (b) draws the flatness, and the dashed and solid lines in purple are power law and the horizontal fitting lines, respectively.

granules with sizes smaller than this value. This indicates that the granules with sizes larger than 600 km are none intermittency but are highly intermittent for granules with sizes smaller than 600 km. Correspondingly, the size distribution for granules with sizes larger than 600 km is fitted well by a Gauss function and that with sizes smaller than 600 km is fitted by a power-law function. The critical size of 600 km here is found at the position where the fitting functions change in size distribution and the position where the structure function starts to change from horizontal tendency to the slope tendency. Then, for the granules with sizes larger than the critical size, they are considered to be dominated by convection, while the small ones are dominated by turbulence because in a stationary dynamical system, in which the fluid elements move with smooth path, the variables keep averagely stable or constant if their probability density functions follow Gauss functions, but do not if they follow power-law distributions (Frisch 1995).

We further calculated the numbers and area coverage of granules with sizes larger and smaller than 600 km, and found that the numbers are 75 and 759 for region A, 103 and 692 for region B, 1183 and 8640 for the whole FOV, respectively. The area coverage is 25% and 14%, 46% and 16%, 46% and 16%, respectively. It is clear to see that the area coverage of small granules that with sizes smaller than 600 km keeps same for regions A, B and the whole FOV, while it is obviously smaller for the large granules in region A than that in region B and in the whole FOV.

4. Discussions

In this work, we applied the granular segmenting algorithm (Liu et al. 2021) to extract and identify granules in an active

region. The algorithm extracts granules by searching the local intensity valleys as edges. Comparing with the granular patterns in panel (a) of Figures 2 and 3, panel (b) of Figures 2 and 3 show good segmenting results, indicating that the algorithm could segment the granules well. Actually, the method of finding the granular edges by detecting the local intensity valleys is reasonable because the edges are in the regions where granules cool down and drop downward. This method could successfully isolate both the large bright and small faint granules, but could not separate those that stay very close to each other and share part of edges. Hereby, step (2) is applied to separate such granules. In order to obtain pure granules, step (3) is taken to first extract all BPs, and then discard them from the segmented cells. The BP identification is mainly taken by the method described in Liu et al. (2018). However, we notice that when selecting BP seeds from the image convolving with Laplace kernel, the threshold varies in different regions. For instance, the threshold taken in plage regions is slightly lower than those in quiet regions. Hence, we cut the whole FOV into four subregions, select proper thresholds to extract BPs, combine and finally remove them from the segmenting results.

There are many different granule segmentation methods developed in previous work (Bovelet & Wiehr 2001; Abramenko et al. 2012; Falco et al. 2017; Roudier et al. 2020). Here we take the one applied in Abramenko et al. (2012) as an example, in which they used multiple intensity thresholds to extract large bright granules, and then separately detected small ones. This could identify granules well, but the detected edges are dependent on the intensity thresholds. The authors presented a group of size distributions which are almost same even they are

derived with a group of different intensity thresholds separately. Liu et al. (2021) obtained a similar size distribution with the data taken by the same instrument but using a different granular segmentation algorithm. This reveals that both granular segmentation methods are reliable, and the detected granules could show their distribution properties even the extracted sizes vary slightly.

Abramenko et al. (2012) fitted the size distributions of granules with the combination of Gauss function and power-law function. They suggested that the granules with sizes larger than 1000 km are regular ones and are dominated by convection, and the ones with sizes smaller than 600 km are dominated by turbulence. However, they did not explain the dynamics of granules in the range between 600 and 1000 km. Liu et al. (2021) filled the gap, who fitted the size distributions with a Gauss function, the combination of Gauss and power-law functions, and a power-law function in three different length ranges, separately, which correspond well to the “flat,” nonlinear line and the slope line in the flatness. Based on this, they separated the granules into three regimes, and explicated the granules in different length ranges by the convection, “transition domain,” and the turbulence, separately.

We compared the size distribution and flatness of granules in the active region with those in quiet regions reported by Liu et al. (2021), and found that there is only one critical point which separates the granules in the active region into two regimes. Namely, these granules in their lifetimes are first convective and then turbulent. The “transition domain” which describes the mixing motions of convection and turbulence exists in quiet regions, however, is absent in the active region. Additionally, the length ranges of the regimes change as well. Liu et al. (2021) gave the turbulent granules in the range of about 130–265 km, the granules in “transition domain” in the range of 265–1420 km, and the regular granules with sizes above 1420 km. In this work, we found the turbulent granules have sizes smaller than 600 km, and convective granules have sizes larger than 600 km. Such a difference is probably caused by the interaction between granules and magnetic fields in the active region.

It is well known that the photospheric magnetic fields move passively under the convective and turbulent motions, but they move slowly and even stay still when they possess a large area with strong magnetic flux densities. The strong magnetic fields cause high magnetic pressures, behave like a wall, create barriers, and prevent the photospheric flows from moving through, leading to the granules expanding in certain directions with high gas pressure gradients. The wall effect on one hand slows down the evolution of granules, leading to the convective granules extending their sizes down to small, like about 600 km, and on the other hand causes wide intergranular lanes that are averagely wider than the ones in quiet regions due to rooting of dense magnetic fields, leading

to the small granules isolated in such wide intergranular lanes being rotated as a whole by strong downflows in surroundings. Probably this is the main reason that results in the absence of “transition domain” for granules in active regions.

5. Conclusion

We extracted and identified granules in an active region near disk center obtained with GST, and analyzed the length scale distribution and flatness of granules. We found that the length scales of granules that possess sizes larger than 600 km follow Gauss function and behave “flat” in flatness, which reveals that these granules are dominated by convective motions. While the length scales of granules with sizes smaller than 600 km follow power-law in both size distribution and flatness, which indicates that the small size granules are dominated by turbulence. Unlike what have been found in quiet region (Liu et al. 2021), there is no “transition domain” between the convection and turbulence. Such a difference between quiet regions and active regions might be attributed to the different magnetic field environment, namely, caused by the interaction between the fluid motions and strong magnetic fields in active regions.

This work provides an important clue on the interaction of photospheric fluid motions and magnetic fields in active regions. During this process, the dynamical energies may be transported into magnetic energies and stored in magnetic field structures, and the dispersion of the magnetic fields may be obviously different from that in quiet regions.

Acknowledgments

We thank the referee very much for all the effort on the paper and all the valuable suggestions and comments. This work is supported by the National Natural Science Foundation of China (Nos. 41822404, 11973083, 42074205, 11763004, 11729301, 11803005, 12111530078 and 12173012) and Shenzhen Technology Project (JCYJ20190806142609035 and GXWD 20201230155427003-20200804151658001). We thank the GST team for providing high quality data. BBSO operation is supported by NJIT and US NSF AGS-1821294 grant. GST operation is partly supported by the Korea Astronomy and Space Science Institute, the Seoul National University, the Key Laboratory of Solar Activities of Chinese Academy of Sciences (CAS) and the Operation, Maintenance and Upgrading Fund of CAS for Astronomical Telescopes and Facility Instruments.

ORCID iDs

Yan-Xiao Liu  <https://orcid.org/0000-0002-3921-1679>
Chao-Wei Jiang  <https://orcid.org/0000-0002-7018-6862>
Ding Yuan  <https://orcid.org/0000-0002-9514-6402>
Ping-Bing Zuo  <https://orcid.org/0000-0003-4711-0306>
Wen-Da Cao  <https://orcid.org/0000-0003-2427-6047>

References

- Abramenko, V., & Yurchyshyn, V. 2010, *ApJ*, 722, 122
- Abramenko, V. I. 2005, *SoPh*, 228, 29
- Abramenko, V. I., Yurchyshyn, V. B., Goode, P. R., Kitiashvili, I. N., & Kosovichev, A. G. 2012, *ApJL*, 756, L27
- Andic, A., Chae, J., & Goode, P. R. 2011, in *Physics of Sun and Star Spots*, ed. D. Prasad Choudhary & K. G. Strassmeier, Vol. 273 (Cambridge: Cambridge University Press), 339
- Bellot Rubio, L., & Orozco Suárez, D. 2019, *LRSP*, 16, 1
- Berger, T. E., & Title, A. M. 2001, *ApJ*, 553, 449
- Bovelet, B., & Wiehr, E. 2001, *SoPh*, 201, 13
- Cao, W., Gorceix, N., Coulter, R., et al. 2010, *AN*, 331, 636
- Caroli, A., Giannattasio, F., Fanfoni, M., et al. 2015, *JPIPh*, 81, 495810514
- Dunn, R. B., & Zirker, J. B. 1973, *SoPh*, 33, 281
- Falco, M., Puglisi, G., Guglielmino, S. L., et al. 2017, *A&A*, 605, A87
- Frisch, U. 1995, *Turbulence: The Legacy of A.N. Kolmogorov* (Cambridge: Cambridge Univ. Press)
- Goode, P. R., & Cao, W. 2012, *Proc. SPIE*, 8444, 844403
- Liu, Y., Chaowei, J., Ding, Y., et al. 2021, *ApJ*, 923, 133
- Liu, Y., Xiang, Y., Erdélyi, R., et al. 2018, *ApJ*, 856, 17
- Lovejoy, S. 1982, *Sci*, 216, 185
- Mandelbrot, B. B. 1977, *The Fractal Geometry of Nature* (New York: W.H. Freeman & Co)
- Narayan, G., & Scharmer, G. B. 2010, *A&A*, 524, A3
- Petrovay, K. 2001, *SSRv*, 95, 9
- Roudier, T., Malherbe, J. M., Gelly, B., et al. 2020, *A&A*, 641, A50
- Roudier, T., & Muller, R. 1986, *SoPh*, 107, 11
- Salucci, G., Bertello, L., Cavallini, F., Ceppatelli, G., & Righini, A. 1994, *A&A*, 285, 322
- Shumko, S., Gorceix, N., Choi, S., et al. 2014, *Proc. SPIE*, 9148, 914835
- Title, A. M., Topka, K. P., Tarbell, T. D., et al. 1992, *ApJ*, 393, 782
- Utz, D., Hanslmeier, A., Möstl, C., et al. 2009, *A&A*, 498, 289
- Wöger, F., & von der Lühe, O. 2007, *ApOpt*, 46, 8015
- Yang, Y., Ji, K., Feng, S., et al. 2015, *ApJ*, 810, 88
- Yang, Y., Li, Q., Ji, K., et al. 2016, *SoPh*, 291, 1089